Novel tumor suppressor roles for *GZMA* and *RASGRP1* in dissemination of both *Theileria annulata*-transformed macrophages and human B-lymphoma cells

Zineb Rchiad[1,2,3*], Malak Haidar[1,2,3*], Hifzur Rahman Ansari[1,4°], Shahin Tajeri[2,3°], Sara Mfarrej[1], Fathia Ben Rached[1], Abhinav Kaushik[1], Gordon Langsley[2,3#], Arnab Pain[1,5#]

[1]Pathogen Genomics Laboratory, BESE Division, King Abdullah University of Science and Technology (KAUST), Thuwal-23955-6900, Saudi Arabia.
[2]Laboratoire de Biologie Cellulaire Comparative des Apicomplexes, Faculté de Médecine, Université Paris Descartes - Sorbonne Paris Cité, France.
[3] Inserm U1016, Cnrs UMR8104, Cochin Institute, Paris, 75014 France.
[4]King Abdullah International Medical Research Center (KAIMRC), King Abdulaziz Medical City, Ministry of National Guard Health Affairs, Jeddah 21423, Saudi Arabia.
[5]Global Station for Zoonosis Control, Global Institution for Collaborative Research and Education (GI-CoRE), Hokkaido University, N20 W10 Kita-ku, Sapporo, Japan.
*Co-first authors; °Co-second authors

Running Title: Role of Key Genes in *Theileria annulata*-mediated Leukocyte Transformation

Key Words: *Theileria annulata*, *RASGRP1*; *GZMA;* Tumor suppressor; Transcriptome

Financial Support: This study was supported by the Competitive Research Grant 4 (OSR-2015-CRG4-2610) from the Office for Sponsored Research in King Abdullah University of Science and Technology (KAUST). ST was supported by a ParaFrap post-doctoral fellowship and GL acknowledges support from Labex ParaFrap (ANR-11-LABX-0024), INSERM and the CNRS.

#Corresponding authors:
Gordon Langsley; Email: gordon.langsley@inserm.fr, 27, rue du Faubourg-Saint-Jacques, 75014 Paris, office: +33-(0)1-40-51-65-92
Arnab Pain; Email: arnab.pain@kaust.edu.sa, 4700 King Abdullah University of Science and Technology, Thuwal 23955 6900, phone: +966 (0) 2808-2561

The authors declare no potential conflict of interest.

This manuscript is a research article composed of a 40 word summary, 160-word abstract, 4390 text word count, 6 figures, 1 table, 7 supplementary figures, 4 supplementary tables and 61 references.

Summary

We compared the transcriptomes of *Theileria annulata* transformed B-lymphocytes to 934 human cancer cell lines and provide functional evidence for shared tumor suppressor roles for GZMA and RASGRP1 in controlling the dissemination phenotype of both human B lymphomas and Theileria-transformed leukocytes.

Abstract

Theileria annulata is a tick-transmitted apicomplexan parasite that infects and transforms bovine leukocytes into disseminating tumors that cause a disease called tropical theileriosis. Using comparative transcriptomics we identified genes transcriptionally perturbed during *Theileria*-induced transformation. Dataset comparisons highlighted a small set of genes associated with *Theileria*-transformed leukocyte dissemination. The roles of Granzyme A (*GZMA*) and RAS guanyl-releasing protein 1 (*RASGRP1*) were verified by CRISPR/Cas9-mediated knock-down. Knocking down of *GZMA* and *RASGRP1* in attenuated macrophages led to a regain in their dissemination in Rag2/γC mice confirming their role as dissemination suppressors *in vivo*. We further evaluated the roles of *GZMA* and *RASGRP1* in human B-lymphoma cells by comparing the transcriptome of 934 human cancer cell lines to that of *Theileria*-transformed bovine host cells. We confirmed dampened dissemination potential of human B-lymphoma cells that overexpress *GZMA* and *RASGRP1*. Our results provide evidence that *GZMA* and *RASGRP1* have a novel tumor suppressor function in both *T. annulata*-infected bovine host cells and in human B-lymphomas.

54 **INTRODUCTION**

55 *Theileria annulata* is a tick-transmitted apicomplexan parasite that infects and
56 transforms bovine leukocytes into disseminating tumors that cause a widespread disease
57 called tropical theileriosis. In countries endemic for tropical theileriosis live attenuated
58 vaccines are produced by multiples *in vitro* passages of virulent, transformed
59 macrophages and vaccination protects animals from severe disease (1). Amazingly the
60 fully transformed state can be completely reversed by drug-induced parasite death making
61 *Theileria*-infected leukocytes a powerful cellular model to identify genes regulating cellular
62 transformation and dissemination (2). This parasite-based reversible model of leukocyte
63 transformation has allowed the identification of several cell signaling pathways associated
64 with the virulence of *Theileria*-transformed leukocytes such as c-Jun NH2-terminal
65 kinase/c-Jun/PI3 kinase signaling (3), protein kinase A (PKA) (4), transforming growth
66 factor beta 2 (TGF-b2) (5) (6) and SMYD3/MMP9 (7). MMP-9 and c-Jun are associated
67 with invasion, proliferation and angiogenesis in *Theileria*-mediated host cell transformation
68 as well as in human cancer (3, 8-10). Epigenetic changes also contribute to *Theileria*-
69 induced leukocyte transformation (12). OncomiR addiction has been described as being
70 generated by a miR-155 feedback loop in *T. annulata*-transformed B cells (13). Similarly,
71 miR-126-5p contributes to infected macrophage dissemination through JNK-Interacting
72 Protein-2 (JIP2)/JNK1/AP1-mediated *MMP9* transcription (14).

73 It's well established that *T. annulata* modulates gene expression of its host cell and
74 hijacks key signalling cascades. For example, RNA extracted from *T. annulata*-
75 transformed B cells was used to screen bovine microarrays demonstrating that infection
76 had reconfigured host cell gene expression (11). Nonetheless, a systematic and genome
77 scale transcriptional comparison of B cells and macrophages transformed by *T. annulata*
78 has been lacking. In this study, we used RNA-seq to define the transcriptional landscapes

79 of two *T. annulata*-transformed B-cell lines and a virulent *T. annulata*-transformed
80 macrophage line (Ode) and the attenuated live vaccine directly derived from it. High
81 stringency bioinformatic comparisons of the transcriptional landscapes identified four
82 candidate genes (*MMP9*, *GZMA*, *RASGRP1* and *SEPP1*) as potential players in the
83 dissemination of virulent *T. annulata*-transformed macrophages.

84 The infection of lymphocytes and macrophages by *Theileria annulata* causes a
85 lymphoproliferative phenotype with properties largely similar to human cancer, most
86 notably immortalization, independence of exogenous growth factors, uncontrolled
87 proliferation and invasiveness. The similarity between *Theileria*-transformed leukocytes
88 and human leukemia suggests that *Theileria-induced transformation* could be a powerful
89 model to elucidate common mechanisms underpinning tumour virulence. In order to
90 generalize our *Theileria*-based observations we compared the transcriptome maps of 934
91 human cancer cell lines to the transcriptomes of *T. annulata* transformed B-lymphocytes
92 and provide functional evidence for shared tumor suppressor roles for *GZMA* and
93 *RASGRP1* in controlling the dissemination phenotype of both human B lymphomas and
94 *Theileria*-transformed leukocytes**.**

95 **Materials and Methods**

96 **Cell lines**

97 The BL3 (15), TBL3, BL20 (16), TBL20 B lymphocytes, and Ode macrophages (17) were
98 cultured in RPMI 1640 medium supplemented with 2 mM of L-glutamine (Lonza,
99 catalogue number 12-702F) and 10 mM Hepes (Lonza, catalogue number 17-737E), 10 %
100 heat-inactivated FBS (Gibco, catalogue number 10082147), 100 units/ml of Penicillin and
101 100 µg/ml of streptomycin (Lonza, catalogue number 17-602E) and 10mM b-
102 mercaptoethanol (Sigma-Aldrich, catalogue number M6250) for BL3/TBL3 and
103 BL20/TBL20. The virulent (Vir) hyper-disseminating Ode cell line was used at low

passage (53-71), while its attenuated (Att) poorly disseminating vaccine counterpart corresponded to passages 309-317. The OCI-LY19 cell line (DSMZ, ACC 528) was cultured in Minimum Essential Medium Eagle - Alpha Modification (Gibco, catalog number 12000063) supplemented with 2.2g/L of sodium bicarbonate (Thermofisher Scientific, catalog number 25080094), 20% FBS, 10 mM Hepes and 100 units/ml of Penicillin and 100 ug/ml of streptomycin. The RI-1 cell line (DSMZ, ACC 585) was cultured in RPMI1640 and supplemented with 10% FBS, 100 units/ml of Penicillin and 100 ug/ml of streptomycin and 10 mM Hepes. All cell lines were incubated at 37°C with 5% CO_2. All cell lines were regularly tested for mycoplasma contamination.

RNA extraction

Cells were seeded in 3 biological replicates at a density of $2.5x10^5$ cell/ml. RNA extraction was performed using the PureLink RNA Mini Kit (Life technologies, catalogue number 12183018A) following the manufacturer's instructions. Briefly, cells were pelleted, lysed and homogenized using a 21-gauge needle, then 70% ethanol was added to the cell lysates and the samples were loaded on spin cartridges to bind RNA. After 3 washes, RNA was eluted in RNase-free water. The quality of extracted RNA was verified using a Bioanalyzer 2100 and quantification carried using Qubit (Invitrogen, catalogue number Q10210).

Illumina library preparation and sequencing

Strand-specific RNA-sequencing (ssRNA-seq) libraries were prepared using the illumina Truseq Stranded mRNA Sample Preparation Kit (Illumina, catalogue number RS-122-2101) following the manufacturer's instructions. Briefly, 1ug of total RNA was used to purify mRNA using poly-T oligo-attached magnetic beads. mRNA was then fragmented and cDNA was synthesized using SuperScript III reverse transcriptase (Thermofisher, catalogue number 18080044), followed by adenylation on the 3' end, barcoding and

129 adapter ligation. The adapter ligated cDNA fragments were then enriched and cleaned
130 with Agencourt Ampure XP beads (Agencourt, catalogue number A63880). Libraries
131 validation was conducted using the 1000 DNA kit on 2100 Bioanalyzer (Agilent
132 Technologies, catalogue number 5067-1504) and quantified using qubit (Thermofisher,
133 catalogue number Q32850). ssRNA libraries were sequenced on Illumina Hiseq2000 and
134 Hiseq4000. The sequenced reads were mapped to the *Bos taurus* genome Btau 4.6.1.
135 The quality of the sequenced libraries is shown in supplementary figure S1.

136 **Sequencing data analysis**

137 The quality of sequence reads and other parameters were checked using FastQC
138 (http://www.bioinformatics.babraham.ac.uk/projects/fastqc/). The raw RNA-seq reads
139 were processed for adaptor trimming by Trimmomatic (19). The strand-specific reads
140 were mapped on to Bovine genome (bosTau7; Btau_4.6.1; GCF_000003205.5) using
141 Tophat2 (-g 1 --library-type fr-firststrand). The samples with respective replicates were
142 analyzed further for differential gene expression by three different tools, baySeq (20),
143 DESeq2 (21) (fitType ="local") and CuffDiff2 (22) with default parameters unless
144 mentioned specifically. The count values for DESeq2 and baySeq were calculated from
145 BAM files using HTSeq-count tool (23). The transcriptome quality plots were generated
146 by cummeRbund package (v2.14.0) in R
147 (http://bioconductor.org/packages/release/bioc/html/cummeRbund.html). The
148 sequencing data is available in the NCBI Gene Expression Omnibus, GEO ID:
149 GSE135377.

150 **Identification of differentially expressed genes after infection and attenuation by**
151 **comparative transcriptome analysis**

152 The transcriptome data was analyzed with baySeq, DESeq2 and CuffDiff2. A gene was
153 considered as a differentially expressed gene (DEG) if it has a padj<0.05 and a fold
154 change (FC)>2. The final list of DEGs contained genes commonly differentially expressed

155 in CuffDiff2, DESeq2 and baySeq. This approach minimalizes the total number of DEGs
156 for further analysis and allows stringent selection of the most significant and reproducible
157 DEGs.

158 **qRT-PCR**

159 Total RNA was reverse transcribed using the High Capacity cDNA Reverse Transcription
160 Kit (Applied Biosystems, catalogue number 4368814) as follows: 2 μg of total RNA, 2 μL
161 of RT buffer, 0.8 μL of 100mM dNTP mix, 2.0 μL of 10X random primers, 1 μL of
162 MultiScribe reverse transcriptase and Nuclease-free water to a final volume of 20 μL. The
163 reaction was incubated 10 min at 25°C, 2 h at 37°C then the enzyme inactivated at 85°C
164 for 5 min. Real time PCR was performed in a 10 μL reaction containing 20-30 ng cDNA
165 template, 5 μL 2X Fast SYBR Green Master Mix and 500 nM of forward and reverse
166 primers. The reaction was run on the 7500 HT Fast Real-Time PCR System (Applied
167 Biosystems). GAPDH was used as a housekeeping gene and the results were analyzed
168 by the $2^{-\Delta\Delta CT}$ method. The error bars represent the SEM of 3 biological replicates. Primers
169 were designed and assessed for secondary structures using the Primer Express Software
170 v3.0. The primers of all genes are listed in Table S3.

171 **Transfection**

172 Macrophages were transfected by electroporation using the Nucleofector system (Amaxa
173 Biosystems). A total of 5×10^5 cells were suspended in 100 μL of Nucleofector V solution
174 mix (Lonza, VCA-1003) with 2 μg of *GZMA* and *RASGRP1* CRISPR/Cas9 plasmids and
175 subjected to nucleofection using the cell line-specific program T-O17. The human B-
176 lymphoma cells were transfected with 2 μg of *GZMA* (SCBT, sc-403958-ACT),
177 *RASGRP1* (SCBT, sc-402120-ACT) and *SEPP1* (SCBT, sc-417457-ACT) activation
178 plasmids, and the non-specific control plasmid (SCBT, sc-437275) using the T-O17

179 program. After transfection, cells were suspended in fresh complete medium and
180 incubated at 37°C with 5% CO_2.

181 **Matrigel chamber assay**

182 The invasive capacity of Ode macrophages was assessed *in vitro* using matrigel migration
183 chambers, as described in (3). The CultureCoat Medium basement membrane extract
184 (BME) 96-wells cell invasion assay was performed according to Culturex instructions
185 (Trevigen, catalog number 3482-096-K). After 24 h of incubation at 37°C, each well of the
186 top chamber was washed once in buffer. The top chamber was placed back onto the
187 receiver plate. One hundred microliters of cell dissociation solution-Calcein AM was added
188 to the bottom chamber of each well, and the mixtures were incubated at 37°C for 1 h with
189 fluorescently labeled cells to dissociate the cells from the membrane before reading at
190 485-nm excitation and 520-nm emission wavelengths.

191 **Soft agar colony forming assay**

192 A two-layer soft agar culture system was used. Cell counts were performed by ImageJ
193 software. A total of 2,500 cells were plated in a volume of 1.5 ml (0.7% bacto Agar+2×
194 RPMI 20% Fetal bovine Serum) over 1.5 ml base layer (1% bacto agar +2× RPMI 20%
195 Fetal bovine Serum) in 6-well plates. Cultures were incubated in humidified 37°C
196 incubators with an atmosphere of 5% CO_2 in air, and control plates were monitored for
197 growth using a microscope. At the time of maximum colony formation (10 days in
198 culture), final colony numbers were counted after fixation with 0.005% Cristal Violet.

199 **Intracellular levels of hydrogen peroxide (H_2O_2)**

200 Cells were seeded at $1x10^5$ cell/well in a 96 well plate and incubated in complete medium
201 for 18 h prior to the assay. Cells were then washed with PBS and incubated with 100 μL
202 of 5 M H2-DCFDA in PBS (Molecular Probes, catalogue number D399). H_2O_2 levels were

203 assayed on a fusion spectrofluorimeter (PackardBell) by spectrofluorimetry at 485 and
204 530nm excitation and emission wavelengths respectively.

205 ***In vivo* mouse studies and quantification of *Theileria annulata*-transformed**
206 **macrophages load in mouse tissues**

207 *T. annulata*-infected macrophage cell lines (Virulent Ode passage 53, attenuated Ode
208 passage 309, attenuated Ode transfected with *RASGRP1* CRISPR/Cas9 knock out
209 plasmid and attenuated Ode transfected with *GZMA* CRISPR/Cas9 knock out plasmid)
210 were injected into four groups of five Rag2γC immunodeficient mice that were equally
211 distributed on the basis of age and sex in each group. The injection site was disinfected
212 with ethanol and one million cells (in 200 µl PBS) were injected under the skin after gentle
213 shaking of the insulin syringe. The mice were kept for 3 weeks and then they were
214 humanely sacrificed and dissected. Six internal organs including heart, lung, spleen,
215 mesentery, left kidney and liver were taken and stored in 500 *µ* L PBS in Eppendorf tubes
216 at -20°C. The tissues were subjected to genomic DNA extraction using the QIAmp DNA
217 mini kit (Qiagen, catalogue number 51304). DNA concentrations were measured by
218 Nanodrop™ 1000 spectrophotometer (Thermo Fischer scientific) and before each
219 quantitative PCR reaction samples were diluted to give a DNA concentration of 0.5 ng/*µ* L.
220 Absolute copy numbers of a single copy *T. annulata* gene (*ama-1*, TA02980) that is
221 representative of *T. annulata*-infected macrophage load in each tissue were estimated by
222 the method described in (24), with some modifications. *ama-1* was cloned into pJET
223 1.2/blunt cloning vector using CloneJET PCR Cloning Kit (Thermo scientific, catalogue
224 number K1232). The cloned plasmid was amplified in DH5-Alpha cells and purified with
225 QIAfilter™ Plasmid Maxi Kit (Qiagen, catalogue number 12243). Plasmid concentration
226 was measured using Qubit (Thermofisher, catalogue number Q32850). The primers for
227 cloning were: forward 5'-GGAGCTAACTCTGACCCTTCG-3'and reverse 5'-

228 CCAAAGTAGGCCAATACGGC-3'. Quantitative PCR primers were: forward 5'-
229 GACCGATTTCATGGCAAAGT-3'and reverse 5'-TTGGGGTCATGATGGGTTAT-3'.

230 **Transcriptome-based clustering of *Theileria*-transformed bovine host cells and**
231 **human cancer cell lines**

232 The processed and quality trimmed reads from TBL20/BL20 and BL3/TBL3 samples
233 were mapped to *Bos taurus* UMD3.1 genome using HISAT2 software (25) with default
234 settings. The mapped reads were used for gene-level TPM quantification using StringTie
235 (Version 1.3.3b) (26, 27). The quantified genes were converted into their human ortholog
236 Ensemble gene ID by finding one-to-one orthologs between human and *B. taurus*
237 genomes using OMA browser (28). Subsequently, TPM values of transcripts expressed
238 across 934 human cancer cell lines were obtained from EBI cancer cell line Expression
239 Atlas (29). The redundant transcripts in the cancer cell line expression set were
240 collapsed using collapseRow function from the WGCNA R package (30). Using the
241 common human ensemble gene ID, gene expression matrices of *B. taurus* and human
242 cell lines were merged together, which was then subjected to hierarchical clustering of
243 samples using HCPC (31) with 3 Principal Components (nPCs), which resulted
244 in 4 broad clusters. The sub-cluster containing the human cancer cell lines along with
245 TBL20/BL20 and BL3/TBL3 were shortlisted for further analysis. Whereby, samples
246 were scanned for similar gene expression profiles by computing the adjacency of each
247 shortlisted sample with the rest of the samples, using adjacency function
248 (method="Distance") from WGCNA R package. The resultant adjacency matrix was then
249 subjected to flashClust (31) program for computing the dendrogram for manual
250 inspection of TBL20/BL20 and BL3/TBL3 containing sub-cluster. A schematic of the
251 used pipeline is presented in Fig. S6. The complete dendrogram of the 934 human
252 cancer cell lines and *Theileria*-tranformed lymphocytes can be viewed in Fig. S7.

253 **Ethics statement**

254 The protocol (12-26) was approved by the ethics committee for animal experimentation of
255 the University of Paris-Descartes (CEEA34.GL.03312). The university ethics committee is
256 registered with the French National Ethics Committee for Animal Experimentation that
257 itself is registered with the European Ethics Committee for Animal Experimentation. The
258 right to perform the mice experiments was obtained from the French National Service for
259 the Protection of Animal Health and satisfied the animal welfare conditions defined by
260 laws (R214-87 to R214-122 and R215-10) and GL was responsible for all animal
261 experimentation, as he holds the French National Animal Experimentation permit with the
262 authorisation number (B-75-1249). This project is also covered by the KAUST IBEC
263 number 19IBEC12.

264 **RESULTS:**

265 **Differentially expressed bovine genes in *T. annulata*-transformed leukocytes**

266 The infection and full transformation of the BL20 cell line with *T. annulata* caused
267 profound transcriptional changes, as previously reported for infected BL20 cells (11).
268 Similarly, infection of BL3 cell with *T. annulata* also provoked changes in host cell gene
269 expression (Fig. S2a). Transcriptional changes between virulent compared to attenuated
270 Ode macrophages are less profound, likely because the macrophages only appear to
271 differ in dissemination potential (Fig. S2a).

272 To identify bovine genes whose transcription is perturbed by transformation and
273 attenuation of dissemination of *T. annulata*-transformed leukocytes we concentrated on
274 the most differentially expressed genes (DEGs) (Fig. 1, Table S1). Many of these genes
275 are annotated as being implicated in cell proliferation and metastasis. Amongst the top
276 five-upregulated transcripts in TBL20 is *MMP9* (matrix metallopeptidase 9), a gene highly

277 expressed in different cancer types and linked to metastasis and angiogenesis (32). *WC1-*
278 *8* is the third most upregulated gene in TBL20 lymphocytes and has been described as
279 being also upregulated in ovarian carcinoma cells (33). The most down-regulated
280 transcripts in TBL20 cells include *LAIR1* (leukocyte associated immunoglobulin like
281 receptor 1) and *VPREB* (pre-B lymphocyte 1). *LAIR1* is a strong inhibitor of natural killer
282 cell-mediated cytotoxicity and an inhibitory receptor, which down-regulates B lymphocyte
283 immunoglobulin and cytokine production (34). Down-regulation of *LAIR-1* was not
284 unexpected, as it's loss of expression is observed during B cell proliferation (35). *ZBTB32*
285 (zinc finger and BTB domain containing 32), *IL21R* (interleukin 21 receptor), and *MMP9*
286 are also among the top five up-regulated transcripts in infected TBL3 B lymphocytes. The
287 five most down-regulated transcripts in TBL3 are *KRT6C* (keratin 6C), *MATK*
288 (megakaryocyte-associated tyrosine kinase), *IGSF9B* (immunoglobulin superfamily
289 member 9B), *A2M* (alpha-2-macroglobulin) and *H2AFY2* (H2A histone family, member
290 Y2). The biological functions of these genes include inhibition of cell growth and
291 proliferation (36), repression of DNA transcription (37) and inhibition of cell adhesion and
292 migration (38), functions that are often dampened to allow continuous proliferation and
293 survival of transformed cells. We confirmed by qRT-PCR differential expression of 21
294 randomly selected genes from the BL20/TBL20 and BL3/TBL3 RNA-seq datasets (Fig.
295 S2b).

296 **Identification of key genes potentially involved in *Theileria*-mediated macrophage**
297 **dissemination**

298 The most down-regulated transcripts in attenuated Ode macrophages are *SKAP2*
299 (src kinase associated phosphoprotein 2), a gene known to promote tumor metastasis
300 through the regulation of podosome formation in macrophages (39) and *NRP2* that

301 regulates tumor progression by promoting TGF-β-signaling (40). Down-regulation of these
302 genes correlates with decreased dissemination of attenuated macrophages, as previously
303 we have described loss of TGF-β-signaling as being associated with decreased
304 dissemination (5). By contrast, the most highly upregulated transcripts include *SEPP1*
305 (selenoprotein P) and *PTPRT* (protein tyrosine phosphatase, receptor type T). Both
306 *SEPP1* and *PTPRT* have been previously described as a tumor suppressor gene (41, 42).
307 Taken together, the identity of the most strongly up- and down-regulated genes argues
308 that our differential transcription screen could identify novel genes regulating *Theileria*-
309 transformed macrophage dissemination.

310 To define the genes likely playing important roles in transformation and
311 dissemination, we compared genes differentially expressed (DE) in TBL3, TBL20 and
312 attenuated Ode macrophages. We assumed that the genes most likely to play a key role
313 are upregulated after infection and downregulated upon attenuation, and vice versa. This
314 approach identified four genes likely to play key roles in the dissemination of *Theileria*-
315 transformed leukocytes (Fig. 2a).

316 The genes are *MMP9, SEPP1, GZMA* and *RASGRP1* and their biological functions have
317 been implicated in metastasis and cell invasion (32), selenium transport (43), peptide
318 cleavage by immune cells (44) and regulation of B cell-development and homeostasis and
319 differentiation (45), respectively (Table 1). Differential expression of these genes was
320 confirmed by qRT-PCR (Fig. 2b). We focused on *GZMA*, *RASGRP1* and *SEPP1*, as the
321 role of *MMP9* in metastasis/dissemination is well established including in *Theileria*-
322 transformed macrophages (46). CRISPR/Cas9-mediated loss of *SEPP1* in attenuated
323 macrophages resulted in a lethal phenotype highlighting its essentiality in transformed
324 macrophage survival and the role of SEPP1 in *Theileria*-transformed cell lines was not
325 further evaluated.

326 **Ablation of *GZMA* and *RASGRP1* by CRISPR/Cas9 knockdown**

327 To confirm a role for *GZMA* and *RASGRP1* in dissemination of *T. annulata*-
328 transformed Ode macrophages, we knocked down their expression by CRISPR/Cas9 and
329 decreased expression led to a regain in dissemination potential, as estimated in matrigel
330 traversal assays (Fig. 3b). Both GZMA and RASGRP1 have therefore, the potential to
331 function as suppressors of tumor dissemination and consistently, knockdown of *GZMA*
332 also led to a regain in the ability of attenuated macrophages to form colonies in soft agar
333 (Fig.3c). Taken together it strongly suggests that GZMA and RASGRP1 function as tumor
334 suppressors.

335 ***GZMA* and *RASGRP1* dampen *in vivo* dissemination of Ode macrophages**

336 Similar to metastatic tumor cells *T. annulata*-transformed leukocytes also
337 disseminate in immuno-deficient mice to distant organs and form proliferative foci (47).
338 Dissemination of *Theileria*-transformed leukocytes has been previously attributed to
339 increased production of matrix metaloproteinases (MMPs) (46). As *GZMA* and *RASGRP1*
340 knockdown led to a regain in matrigel traversal we used Rag2γC immunodeficient mice to
341 test for a regain in dissemination *in vivo*. The CRISPR/Cas9-induced ablation of
342 expression of GZMA and RASGRP1 gave rise to an increase in the number of *Theileria*-
343 containing tumors in heart, lung and mesentery, while knockdown of *RASGRP1* increased
344 the number of tumors in the liver (Fig. 4). Thus, loss of *RASGRP1* and *GZMA* expression
345 led to a regain in the invasive capacity of *T. annulata*-transformed macrophages into these
346 organs.

347 **Induced expression of *GZMA*, *RASGRP1* and *SEPP1* reduces human B-lymphoma**
348 **cell dissemination**

349 In order to extend the roles of GZMA, RASGRP1 and SEPP1 to human cancer we
350 sought human tumor cells displaying transcriptional signatures similar to *T. annulata*-
351 transformed leukocytes. To this end, the transcriptional profiles of 934 human cancer cells
352 were obtained from the EBI cancer cell line expression atlas (29) and their profiles
353 compared to those of *Theileria*-transformed TBL3 and TBL20 B-lymphocytes (Fig. 5a).
354 Among the subset human B lymphomas OCI-LY19 and RI-1 displayed the transcriptional
355 signature most similar to TBL3 and TBL20 and therefore, were used to test if *GZMA,*
356 *RASGRP1* and *SEPP1* can act as suppressors of dissemination in certain types of human
357 cancer. CRISPR-mediated transcriptional activation of *GZMA*, *RASGRP1* and *SEPP1*
358 resulted in decreased matrigel traversal of the OCI-LY19 B lymphoma. By contrast, only
359 upregulation of *GZMA* showed a statistically significant decrease in traversal of the RI-1 B
360 lymphoma (Fig. 5c). Clearly, *GZMA* has the potential to act as a suppressor in two
361 independent human B-lymphomas, whereas *RASGRP1* and *SEPP1* may only function as
362 suppressors in specific B-lymphomas.

363 **DISCUSSION**

364 In this study, we provide a holistic view of the transcriptional landscape of two *T.*
365 *annulata*-transformed B cell lines, TBL3 and TBL20, and in addition the landscape of
366 virulent versus attenuated Ode macrophages. In order to find genes with commonly
367 perturbed transcription the different datasets were compared using three independent
368 pipelines to identify just four genes, as potential regulators of tumor dissemination. In
369 addition to *MMP9* three other genes (*SEPP1*, *GZMA* and *RASGRP1*) were identified as
370 potentially having a role in dissemination. SEPP1 is a major selenoprotein involved in
371 selenium transport and cellular defense against oxidative stress (48). Attenuated

372 macrophages did not survive CRISPR/Cas9-knockdown of *SEPP1* implying death might
373 be due to a failure to control excessive oxidative stress, since attenuated macrophages
374 display high levels of H_2O_2 (49).

375 RASGRP1-activated Ras family proteins possess both pro- and anti-oncogenic
376 properties, depending on the downstream effector pathway and cellular context; reviewed
377 in (50). Our transcription profiling showed that most of the members of the *RASGRP* gene
378 family (*RASGRP1, 2 & 4*) are significantly downregulated in TBL3 and TBL20 (Fig. S3).
379 GZMA is a serine protease that contributes to killing of both tumors and pathogen-infected
380 cells via a caspase-independent pathway (44). *GZMA* expression induces reactive oxygen
381 species (51) and attenuated macrophages are known to be more oxidatively stressed than
382 virulent macrophages (49). Indeed, H_2O_2 output was reduced in attenuated macrophages
383 following CRISPR/Cas9-mediated *GZMA* knockdown (Fig. S4). Furthermore, it has been
384 shown that *RASGRP1*-deficient CD8 T cells exhibit markedly reduced expression of
385 GZMB (52) . This led us to investigate whether loss of *RASGRP1* could perhaps provoke
386 a drop in *GZMA* expression rendering attenuated macrophages doubly deficient in
387 dissemination *in vivo*. As hypothesized, we found that expression of *GZMA* decreased
388 after *RASGRP1* knockdown (Fig. S5). Moreover, *GZMA* and *RASGRP1* expression is
389 repressed by TGF-β (52, 53) and the role of TGF-β in regulating dissemination of
390 *Theileria*-transformed macrophages is very well established (4-6). Expression of *GZMA*
391 and *RASGRP1* was decreased in attenuated Ode macrophages treated with TGF-β
392 (Table S4). Taken altogether, it suggests that one way TGF-β promotes dissemination of
393 *Theileria*-transformed leukocytes could be via repression of both *GZMA* and *RASGRP1*
394 transcription and their impact on dissemination confirmed *in vivo* in mice. In addition to the
395 role of *GZMA, RASGRP1* and *SEPP1* in regulating tumorigenesis of *Theileria*-transformed
396 leukocytes, all three genes also dampened the capacity of the human OCI-LY19 B-

397 lymphoma to traverse matrigel and GZMA also dampened traversal of human RI-1 B
398 lymphoma cells.

399 GZMA is known to cleave APEX1 (apurinic/apyrimidinic endodeoxyribonuclease 1)
400 after Lys31 and destroys its oxidative repair functions. APEX1 is involved in NK-cell-
401 mediated killing via GZMA (51, 54) and can suppress the activation of PARP1 during
402 repair of oxidative DNA damage (55), and prevent oxidative stress by negatively
403 regulating Rac1/GTPase activity (56). Additionally, APEX1 directly reduces the redox-
404 sensitive cysteine residues of target transcription factors, enhancing their DNA binding
405 and transcriptional activity. Analysis of our deep RNA-seq data revealed that *APEX1* is
406 downregulated in attenuated macrophages and its expression increases after TGF-β
407 treatment, along with an important downregulation of *GZMA* and *RASGRP1* (Table S4). It
408 is over-expressed in many cancers (57) (58) (59) and has been implicated in growth,
409 migration and invasion of colon cancer both *in vitro* and *in vivo* (60). Interestingly, APEX-1
410 protects melanoma cells from H_2O_2 induced apoptosis (57). The established function of
411 APEX1 in human cancer sustains our novel observations on the tumor suppressor roles of
412 *GZMA* and *RASGRP1.* The ensemble of our results allows us to propose a model, where
413 TGF-β modulates tumor redox balance-mediated dissemination by regulating a
414 GZMA/RASGRP1/APEX1 pathway (Fig. 6).

415 This study has revealed new players in dissemination and oxidative stress regulation of
416 *Theileria*-transformed leukocytes and has provided evidence for similar roles for GZMA
417 and RASGRP1 in transcriptionally matched human B-lymphoma cell lines. The similarity
418 between *Theileria*-induced B cell transformation and human B-lymphomas has unveiled
419 novel therapeutic targets to treat cancer.

Acknowledgements.

This study was supported by a Competitive Research Grant from the Office for Sponsored Research (OSR-2015-CRG4-2610) at King Abdullah University of Science and Technology (KAUST) awarded to AP and GL. ZR acknowledges KAUST for awarding her PhD studentship. ST was supported by a post-doctoral fellowship from ParaFrap (ANR-11-LABX-0024) and in addition to ANR-11-LABX-0024 GL also acknowledges core support from INSERM and the CNRS. We thank members of the Bioscience Core Laboratory (BCL) at KAUST for producing the raw sequencing datasets. Franck Letourneur of the genomics platform at the Cochin institute (GENOM'IC) for quantifying the pJET-*ama-1* plasmid.

Author contributions.

AP and GL conceived and designed the study. ZR prepared the ssRNAseq libraries, SM, MH and ZR ran qRT-PCR reactions. MH performed the soft agar colony formation assay, intracellular H_2O_2 levels and invasion assays. ST performed the mouse dissemination assays, HRA, AK and ZR performed data analysis. ZR and MH prepared the figures and ZR prepared the first draft of the manuscript with input from FBR that was then edited by MH, GL and AP.

437 **References**

438 1. **Nene V, Morrison WI.** 2016. Approaches to vaccination against Theileria
439 parva and Theileria annulata. Parasite Immunol **38:**724-734.
440 2. **Tretina K, Gotia HT, Mann DJ, Silva JC.** 2015. Theileria-transformed bovine
441 leukocytes have cancer hallmarks. Trends Parasitol **31:**306-314.
442 3. **Lizundia R, Chaussepied M, Huerre M, Werling D, Di Santo JP, Langsley**
443 **G.** 2006. c-Jun NH2-terminal kinase/c-Jun signaling promotes survival and
444 metastasis of B lymphocytes transformed by Theileria. Cancer Res **66:**6105-
445 6110.
446 4. **Haidar M, Echebli N, Ding Y, Kamau E, Langsley G.** 2015. Transforming
447 growth factor beta2 promotes transcription of COX2 and EP4, leading to a
448 prostaglandin E2-driven autostimulatory loop that enhances virulence of
449 Theileria annulata-transformed macrophages. Infect Immun **83:**1869-1880.
450 5. **Chaussepied M, Janski N, Baumgartner M, Lizundia R, Jensen K, Weir W,**
451 **Shiels BR, Weitzman JB, Glass EJ, Werling D, Langsley G.** 2010. TGF-b2
452 induction regulates invasiveness of Theileria-transformed leukocytes and
453 disease susceptibility. PLoS Pathog **6:**e1001197.
454 6. **Haidar M, Whitworth J, Noe G, Liu WQ, Vidal M, Langsley G.** 2015. TGF-
455 beta2 induces Grb2 to recruit PI3-K to TGF-RII that activates JNK/AP-1-
456 signaling and augments invasiveness of Theileria-transformed macrophages.
457 Sci Rep **5:**15688.
458 7. **Cock-Rada AM, Medjkane S, Janski N, Yousfi N, Perichon M, Chaussepied**
459 **M, Chluba J, Langsley G, Weitzman JB.** 2012. SMYD3 promotes cancer
460 invasion by epigenetic upregulation of the metalloproteinase MMP-9. Cancer
461 Res **72:**810-820.
462 8. **Hofmann UB, Westphal JR, Van Muijen GN, Ruiter DJ.** 2000. Matrix
463 metalloproteinases in human melanoma. J Invest Dermatol **115:**337-344.
464 9. **Vleugel MM, Greijer AE, Bos R, van der Wall E, van Diest PJ.** 2006. c-Jun
465 activation is associated with proliferation and angiogenesis in invasive breast
466 cancer. Hum Pathol **37:**668-674.
467 10. **Adamson R, Logan M, Kinnaird J, Langsley G, Hall R.** 2000. Loss of matrix
468 metalloproteinase 9 activity in Theileria annulata-attenuated cells is at the
469 transcriptional level and is associated with differentially expressed AP-1
470 species. Mol Biochem Parasitol **106:**51-61.
471 11. **Kinnaird JH, Weir W, Durrani Z, Pillai SS, Baird M, Shiels BR.** 2013. A
472 Bovine Lymphosarcoma Cell Line Infected with Theileria annulata Exhibits
473 an Irreversible Reconfiguration of Host Cell Gene Expression. PLoS One
474 **8:**e66833.
475 12. **Robert McMaster W, Morrison CJ, Kobor MS.** 2016. Epigenetics: A New
476 Model for Intracellular Parasite-Host Cell Regulation. Trends Parasitol
477 **32:**515-521.
478 13. **Marsolier J, Pineau S, Medjkane S, Perichon M, Yin Q, Flemington E,**
479 **Weitzman MD, Weitzman JB.** 2013. OncomiR addiction is generated by a
480 miR-155 feedback loop in Theileria-transformed leukocytes. PLoS Pathog
481 **9:**e1003222.

482 14. **Haidar M, Rchiad Z, Ansari HR, Ben-Rached F, Tajeri S, Latre De Late P,**
483 **Langsley G, Pain A.** 2018. miR-126-5p by direct targeting of JNK-interacting
484 protein-2 (JIP-2) plays a key role in Theileria-infected macrophage virulence.
485 PLoS Pathog **14:**e1006942.
486 15. **Theilen GH, Rush JD, Nelson-Rees WA, Dungworth DL, Munn RJ, Switzer**
487 **JW.** 1968. Bovine leukemia: establishment and morphologic characterization
488 of continuous cell suspension culture, BL-1. J Natl Cancer Inst **40:**737-749.
489 16. **Morzaria SP, Roeder PL, Roberts DH, Chasey D, Drew TW.** 1984.
490 Characteristics of a continuous suspension cell line (BL20) derived from a
491 calf with sporadic bovine leukosis.
492 17. **Singh S, Khatri N, Manuja A, Sharma RD, Malhotra DV, Nichani AK.** 2001.
493 Impact of field vaccination with a Theileria annulata schizont cell culture
494 vaccine on the epidemiology of tropical theileriosis. Vet Parasitol **101:**91-
495 100.
496 18. **Goh S, Ngugi D, Lizundia R, Hostettler I, Woods K, Ballingall K, MacHugh**
497 **ND, Morrison WI, Weir W, Shiels B, Werling D.** 2016. Identification of
498 Theileria lestoquardi Antigens Recognized by CD8+ T Cells. PLoS One
499 **11:**e0162571.
500 19. **Bolger AM, Lohse M, Usadel B.** 2014. Trimmomatic: a flexible trimmer for
501 Illumina sequence data. Bioinformatics **30:**2114-2120.
502 20. **Hardcastle TJ, Kelly KA.** 2010. baySeq: empirical Bayesian methods for
503 identifying differential expression in sequence count data. BMC
504 Bioinformatics **11:**422.
505 21. **Kim D, Pertea G, Trapnell C, Pimentel H, Kelley R, Salzberg SL.** 2013.
506 TopHat2: accurate alignment of transcriptomes in the presence of insertions,
507 deletions and gene fusions. Genome Biol **14:**R36.
508 22. **Trapnell C, Hendrickson DG, Sauvageau M, Goff L, Rinn JL, Pachter L.**
509 2013. Differential analysis of gene regulation at transcript resolution with
510 RNA-seq. Nat Biotechnol **31:**46-53.
511 23. **Anders S, Pyl PT, Huber W.** 2015. HTSeq--a Python framework to work with
512 high-throughput sequencing data. Bioinformatics **31:**166-169.
513 24. **Gotia HT, Munro JB, Knowles DP, Daubenberger CA, Bishop RP, Silva JC.**
514 2016. Absolute Quantification of the Host-To-Parasite DNA Ratio in Theileria
515 parva-Infected Lymphocyte Cell Lines. PLoS One **11:**e0150401.
516 25. **Kim D, Langmead B, Salzberg SL.** 2015. HISAT: a fast spliced aligner with
517 low memory requirements. Nat Methods **12:**357-360.
518 26. **Pertea M, Kim D, Pertea GM, Leek JT, Salzberg SL.** 2016. Transcript-level
519 expression analysis of RNA-seq experiments with HISAT, StringTie and
520 Ballgown. Nat Protoc **11:**1650-1667.
521 27. **Pertea M, Pertea GM, Antonescu CM, Chang TC, Mendell JT, Salzberg SL.**
522 2015. StringTie enables improved reconstruction of a transcriptome from
523 RNA-seq reads. Nat Biotechnol **33:**290-295.
524 28. **Altenhoff AM, Glover NM, Train CM, Kaleb K, Warwick Vesztrocy A,**
525 **Dylus D, de Farias TM, Zile K, Stevenson C, Long J, Redestig H, Gonnet**
526 **GH, Dessimoz C.** 2018. The OMA orthology database in 2018: retrieving

527 evolutionary relationships among all domains of life through richer web and
528 programmatic interfaces. Nucleic Acids Res **46:**D477-D485.
529 29. **Papatheodorou I, Fonseca NA, Keays M, Tang YA, Barrera E, Bazant W,**
530 **Burke M, Fullgrabe A, Fuentes AM, George N, Huerta L, Koskinen S,**
531 **Mohammed S, Geniza M, Preece J, Jaiswal P, Jarnuczak AF, Huber W,**
532 **Stegle O, Vizcaino JA, Brazma A, Petryszak R.** 2018. Expression Atlas: gene
533 and protein expression across multiple studies and organisms. Nucleic Acids
534 Res **46:**D246-D251.
535 30. **Langfelder P, Horvath S.** 2008. WGCNA: an R package for weighted
536 correlation network analysis. BMC Bioinformatics **9:**559.
537 31. **Lê S, Josse J, Husson F.** 2008. FactoMineR: An R Package for Multivariate
538 Analysis. 2008 **25:**18.
539 32. **Yu Q, Stamenkovic I.** 2000. Cell surface-localized matrix metalloproteinase-
540 9 proteolytically activates TGF-beta and promotes tumor invasion and
541 angiogenesis. Genes Dev **14:**163-176.
542 33. **Mangala LS, Zuzel V, Schmandt R, Leshane ES, Halder JB, Armaiz-Pena**
543 **GN, Spannuth WA, Tanaka T, Shahzad MM, Lin YG, Nick AM, Danes CG,**
544 **Lee JW, Jennings NB, Vivas-Mejia PE, Wolf JK, Coleman RL, Siddik ZH,**
545 **Lopez-Berestein G, Lutsenko S, Sood AK.** 2009. Therapeutic Targeting of
546 ATP7B in Ovarian Carcinoma. Clin Cancer Res **15:**3770-3780.
547 34. **Merlo A, Tenca C, Fais F, Battini L, Ciccone E, Grossi CE, Saverino D.** 2005.
548 Inhibitory receptors CD85j, LAIR-1, and CD152 down-regulate
549 immunoglobulin and cytokine production by human B lymphocytes. Clin
550 Diagn Lab Immunol **12:**705-712.
551 35. **van der Vuurst de Vries AR, Clevers H, Logtenberg T, Meyaard L.** 1999.
552 Leukocyte-associated immunoglobulin-like receptor-1 (LAIR-1) is
553 differentially expressed during human B cell differentiation and inhibits B
554 cell receptor-mediated signaling. Eur J Immunol **29:**3160-3167.
555 36. **Kim SO, Avraham S, Jiang S, Zagozdzon R, Fu Y, Avraham HK.** 2004.
556 Differential expression of Csk homologous kinase (CHK) in normal brain and
557 brain tumors. Cancer **101:**1018-1027.
558 37. **Perche PY, Vourc'h C, Konecny L, Souchier C, Robert-Nicoud M, Dimitrov**
559 **S, Khochbin S.** 2000. Higher concentrations of histone macroH2A in the Barr
560 body are correlated with higher nucleosome density. Curr Biol **10:**1531-
561 1534.
562 38. **Kurz S, Thieme R, Amberg R, Groth M, Jahnke HG, Pieroh P, Horn LC,**
563 **Kolb M, Huse K, Platzer M, Volke D, Dehghani F, Buzdin A, Engel K,**
564 **Robitzki A, Hoffmann R, Gockel I, Birkenmeier G.** 2017. The anti-
565 tumorigenic activity of A2M-A lesson from the naked mole-rat. PLoS One
566 **12:**e0189514.
567 39. **Tanaka M, Shimamura S, Kuriyama S, Maeda D, Goto A, Aiba N.** 2016.
568 SKAP2 Promotes Podosome Formation to Facilitate Tumor-Associated
569 Macrophage Infiltration and Metastatic Progression. Cancer Res **76:**358-369.
570 40. **Grandclement C, Pallandre JR, Valmary Degano S, Viel E, Bouard A,**
571 **Balland J, Remy-Martin JP, Simon B, Rouleau A, Boireau W, Klagsbrun M,**
572 **Ferrand C, Borg C.** 2011. Neuropilin-2 expression promotes TGF-beta1-

573 mediated epithelial to mesenchymal transition in colorectal cancer cells.
574 PLoS One **6:**e20444.
575 41. **Scott A, Wang Z.** 2011. Tumour suppressor function of protein tyrosine
576 phosphatase receptor-T. Biosci Rep **31:**303-307.
577 42. **Short SP, Whitten-Barrett C, Williams CS.** 2016. Selenoprotein P in colitis-
578 associated carcinoma. Mol Cell Oncol **3:**e1075094.
579 43. **Burk RF, Hill KE, Awad JA, Morrow JD, Kato T, Cockell KA, Lyons PR.**
580 1995. Pathogenesis of diquat-induced liver necrosis in selenium-deficient
581 rats: assessment of the roles of lipid peroxidation and selenoprotein P.
582 Hepatology **21:**561-569.
583 44. **Chowdhury D, Lieberman J.** 2008. Death by a thousand cuts: granzyme
584 pathways of programmed cell death. Annu Rev Immunol **26:**389-420.
585 45. **Priatel JJ, Chen X, Zenewicz LA, Shen H, Harder KW, Horwitz MS, Teh HS.**
586 2007. Chronic immunodeficiency in mice lacking RasGRP1 results in CD4 T
587 cell immune activation and exhaustion. J Immunol **179:**2143-2152.
588 46. **Somerville RP, Adamson RE, Brown CG, Hall FR.** 1998. Metastasis of
589 Theileria annulata macroschizont-infected cells in scid mice is mediated by
590 matrix metalloproteinases. Parasitology **116 (Pt 3):**223-228.
591 47. **Fell AH, Preston PM, Ansell JD.** 1990. Establishment of Theileria-infected
592 bovine cell lines in scid mice. Parasite Immunol **12:**335-339.
593 48. **Hill KE, Dasouki M, Phillips JA, 3rd, Burk RF.** 1996. Human selenoprotein
594 P gene maps to 5q31. Genomics **36:**550-551.
595 49. **Metheni M, Echebli N, Chaussepied M, Ransy C, Chereau C, Jensen K,**
596 **Glass E, Batteux F, Bouillaud F, Langsley G.** 2014. The level of H(2)O(2)
597 type oxidative stress regulates virulence of Theileria-transformed leukocytes.
598 Cell Microbiol **16:**269-279.
599 50. **Cox AD, Der CJ.** 2003. The dark side of Ras: regulation of apoptosis.
600 Oncogene **22:**8999-9006.
601 51. **Martinvalet D, Zhu P, Lieberman J.** 2005. Granzyme A induces caspase-
602 independent mitochondrial damage, a required first step for apoptosis.
603 Immunity **22:**355-370.
604 52. **Thomas DA, Massague J.** 2005. TGF-beta directly targets cytotoxic T cell
605 functions during tumor evasion of immune surveillance. Cancer Cell **8:**369-
606 380.
607 53. **Takami M, Cunha C, Motohashi S, Nakayama T, Iwashima M.** 2018. TGF-
608 beta suppresses RasGRP1 expression and supports regulatory T cell
609 resistance against p53-induced CD28-dependent T-cell apoptosis. Eur J
610 Immunol **48:**1938-1943.
611 54. **Fan Z, Beresford PJ, Zhang D, Xu Z, Novina CD, Yoshida A, Pommier Y,**
612 **Lieberman J.** 2003. Cleaving the oxidative repair protein Ape1 enhances cell
613 death mediated by granzyme A. Nat Immunol **4:**145-153.
614 55. **Peddi SR, Chattopadhyay R, Naidu CV, Izumi T.** 2006. The human
615 apurinic/apyrimidinic endonuclease-1 suppresses activation of poly(adp-
616 ribose) polymerase-1 induced by DNA single strand breaks. Toxicology
617 **224:**44-55.

618 56. **Ozaki M, Suzuki S, Irani K.** 2002. Redox factor-1/APE suppresses oxidative
619 stress by inhibiting the rac1 GTPase. FASEB J **16:**889-890.
620 57. **Yang S, Irani K, Heffron SE, Jurnak F, Meyskens FL, Jr.** 2005. Alterations in
621 the expression of the apurinic/apyrimidinic endonuclease-1/redox factor-1
622 (APE/Ref-1) in human melanoma and identification of the therapeutic
623 potential of resveratrol as an APE/Ref-1 inhibitor. Mol Cancer Ther **4:**1923-
624 1935.
625 58. **Moore DH, Michael H, Tritt R, Parsons SH, Kelley MR.** 2000. Alterations in
626 the expression of the DNA repair/redox enzyme APE/ref-1 in epithelial
627 ovarian cancers. Clin Cancer Res **6:**602-609.
628 59. **Kakolyris S, Kaklamanis L, Engels K, Fox SB, Taylor M, Hickson ID,**
629 **Gatter KC, Harris AL.** 1998. Human AP endonuclease 1 (HAP1) protein
630 expression in breast cancer correlates with lymph node status and
631 angiogenesis. Br J Cancer **77:**1169-1173.
632 60. **Kim MH, Kim HB, Yoon SP, Lim SC, Cha MJ, Jeon YJ, Park SG, Chang IY,**
633 **You HJ.** 2013. Colon cancer progression is driven by APEX1-mediated
634 upregulation of Jagged. J Clin Invest doi:10.1172/JCI65521.
635 61. **Barrett CW, Reddy VK, Short SP, Motley AK, Lintel MK, Bradley AM,**
636 **Freeman T, Vallance J, Ning W, Parang B, Poindexter SV, Fingleton B,**
637 **Chen X, Washington MK, Wilson KT, Shroyer NF, Hill KE, Burk RF,**
638 **Williams CS.** 2015. Selenoprotein P influences colitis-induced tumorigenesis
639 by mediating stemness and oxidative damage. J Clin Invest **125:**2646-2660.

640 **Table 1: Biological functions of DEGs potentially playing key roles in *T. annulata*-**
641 **mediated leukocyte transformation and dissemination**

Gene symbol	Log2 FC (TBL20)	Adj p value	Log2 FC (TBL3)	Adj p value	Log2 FC (ATT)	Adj p value	Biological functions	References on biological functions
MMP9	8.87	0	8.29	0	-2.13	5.14 E-94	Metastasis formation, cancer cells invasion	(32)
SEPP1	-3.95	8.74 E-174	-1.54	3.75 E-248	2.63	1.01 E-140	Transports selenoprotein, tumor suppressor	(48), (42), (61)
GZMA	-2.87	1.45 E-05	-2.25	1.97 E-41	1.02	9.14 E-21	Plays a role in killing pathogen infected cells and cancer cells, induces increase in ROS	(44), (51)
RASGRP1	-3.55	0	-1.78	1.97 E-41	1.2	2.15 E-15	Required for correct functioning of lymphocytes in chronic infections,	(45)

Figure 1

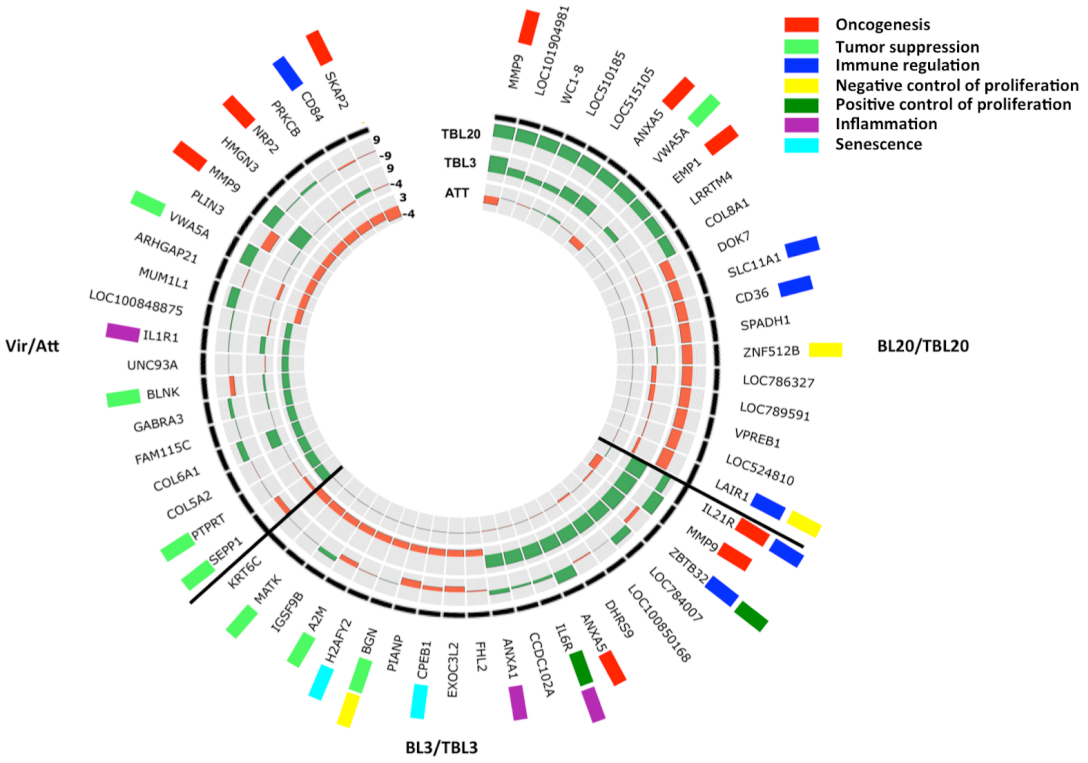

Figure 1: Top 20 differentially expressed genes in Theileria-transformed bovine host cells. A Circos plot showing the top 10 up- and down-regulated DEGs in BL3/TBL3, BL20/TBL20 and Attenuated versus Virulent (Att/Vir) Ode macrophages. The circular heatmap represents the FC of the top DE genes in BL20/TBL20, BL3/TBL3, and Att/Vir Ode in the outer, middle and inner rings, respectively, where green reflects the level of up-regulation and red down-regulation. The genes with biological functions related to tumorigenesis and immune regulation are tagged with colored rectangles. Genes with no tag are hypothetical genes or have no known function in tumorigenesis and immune regulation.

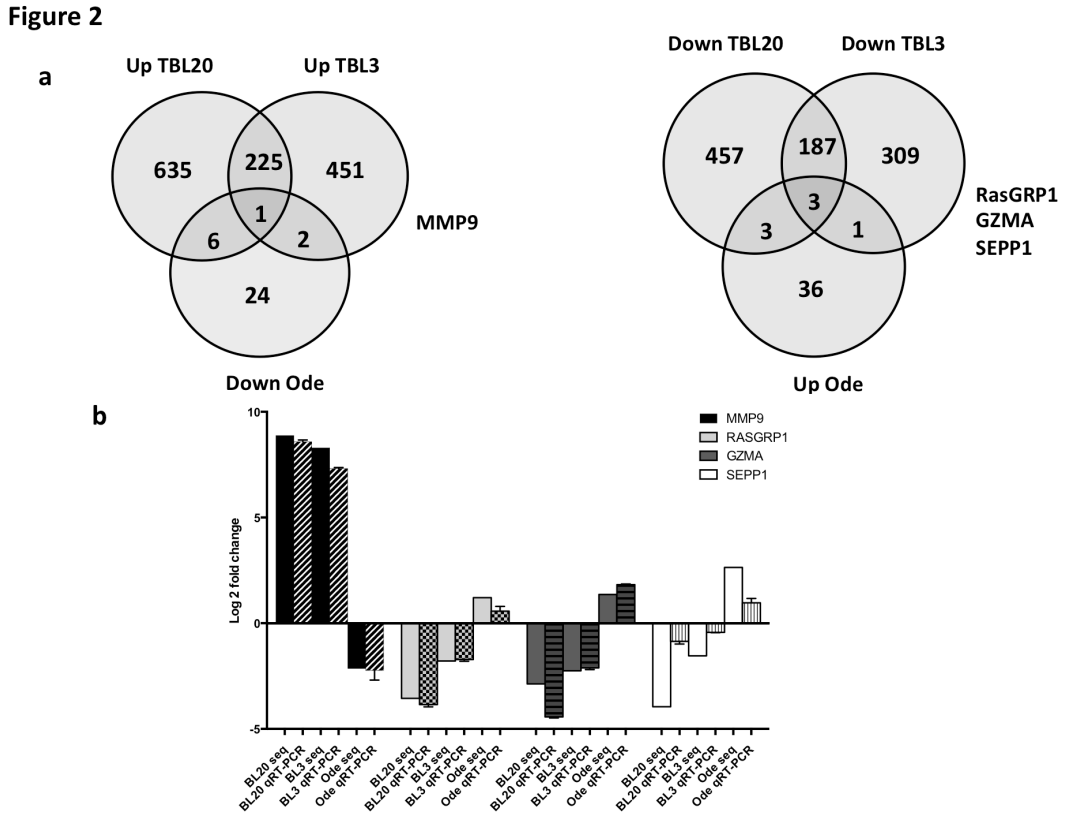

Figure 2: Inversely DEGs in TBL20, TBL3 and Att Ode leukocytes. (a) Venn diagrams illustrating the genes inversely DE in TBL3, TBL20 and Attenuated Ode macrophages. (b) qRT-PCR confirmation of DEGs potentially playing key roles in leukocyte transformation and dissemination. The reactions were set in 3 biological replicates and the fold-change calculated with the $2^{\Delta\Delta ct}$ method. The error bars represent SEM.

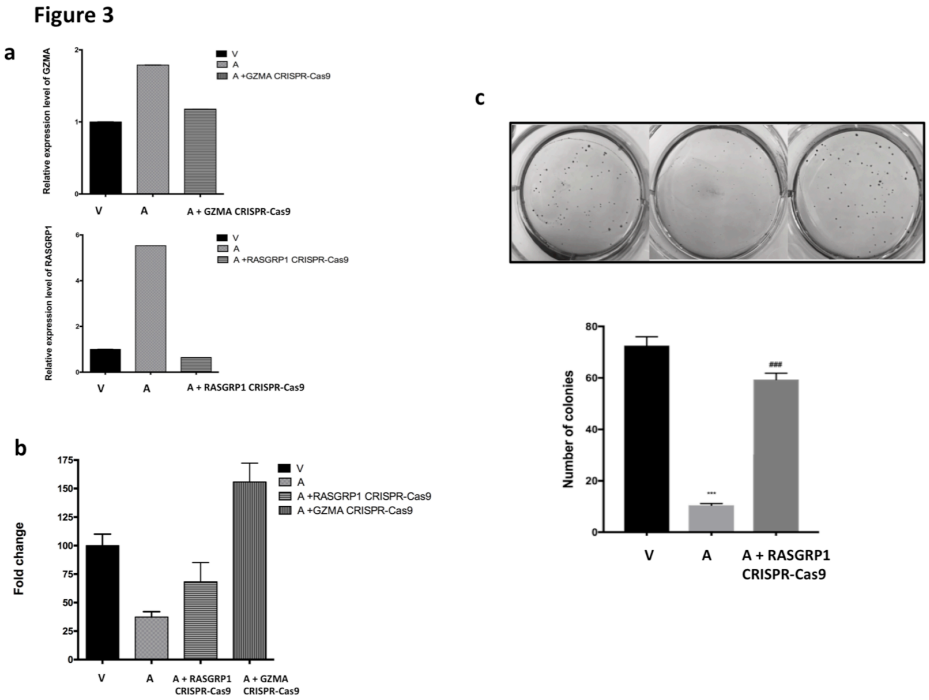

Figure 3: Colony formation on soft agar. (a) qRT-PCR confirmation of *GZMA* (top panel) and *RASGRP1* (bottom panel) knockdown. b) Matrigel chamber assay showing a regain in Matrigel traversal after *RASGRP1* and *GZMA* knockdown. c) Increased colony formation in soft agar following *RASGRP1* knockdown. Non-transfected virulent disseminating Ode macrophages are indicated by V, and non-transfected poorly disseminating attenuated Ode macrophages by A. Error bars represent SD of 3 biological replicates. *** and ### represent student t test $p<0.001$ compared to virulent and attenuated Ode macrophages, respectively.

Figure 4

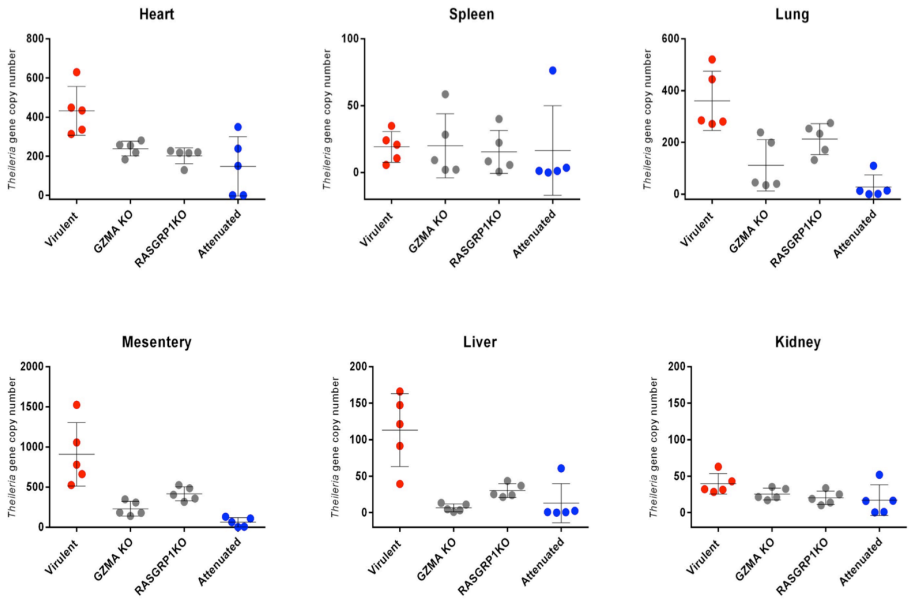

664 **Figure 4: Effect of *GZMA* and *RASGRP1* knockdown on transformed macrophage**
665 **dissemination *in vivo*.** Panels represent the copy number of the single copy *T. annulata*
666 gene (*ama-1*, TA02980) in six internal organs: heart, lung, spleen, mesentery, left kidney
667 and liver. Transformed macrophages were injected into five Rag2γC immunodeficient
668 mice and plotted values represent the mean of obtained *T. annulata*-specific *ama1* gene
669 copy number. Error bars represent SD of 5 biological replicates.

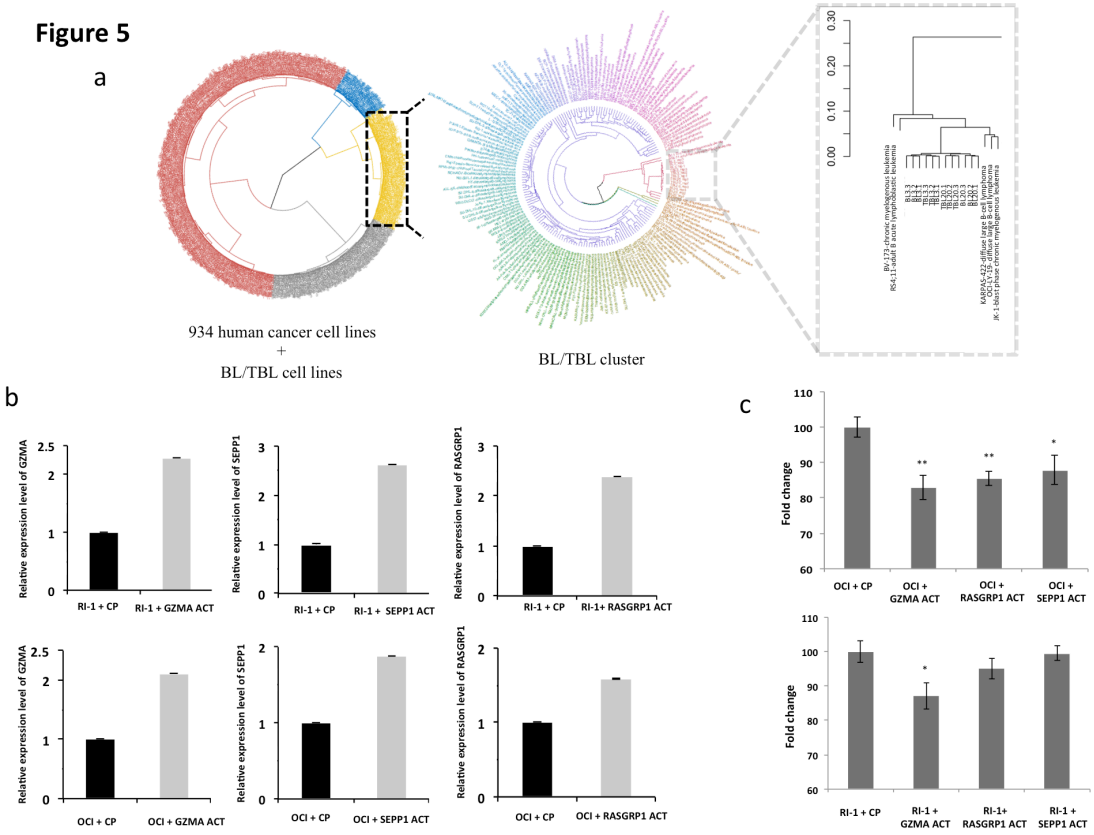

Figure 5: Effect of GZMA, RASGRP1 and SEPP1 activation on human B-lymphomas. (a) (Left panel) PCA based hierarchical clustering of 934 human cancer cell lines and *T. annulata*-transformed bovine B cells and their non-infected counterparts. The cluster containing bovine cells mainly contains leukemic human cancer cell lines. The samples are colored by cluster ID. (Middle cluster) The samples from the BL3/TBL3 and BL20/TBL20 sub-cluster were re-clustered by comparing the similarity of their gene expression profiles. The sample labels are colored by their similarity to each other. (Right panel) The sub-cluster containing bovine cell lines and human cancer cell lines with similar gene expression profile. (b) qRT-PCR determination of *GZMA*, *RASGRP1* and *SEPP1* expression after CRISPR-mediated gene activation in RI-1 (top panel) and OCI-LY19 (bottom panel). The error bars represent SEM of 3 biological replicates. (c) Matrigel chamber assay illustrating the dissemination potential of RI-1 and OCI-LY19

682 following activation of *RASGRP1* and *GZMA* transcription. Errors bars represent SEM
683 values of 3 biological replicates * and ** represent student t test $p<0.05$ and $p<0.005$,
684 respectively.

Figure 6

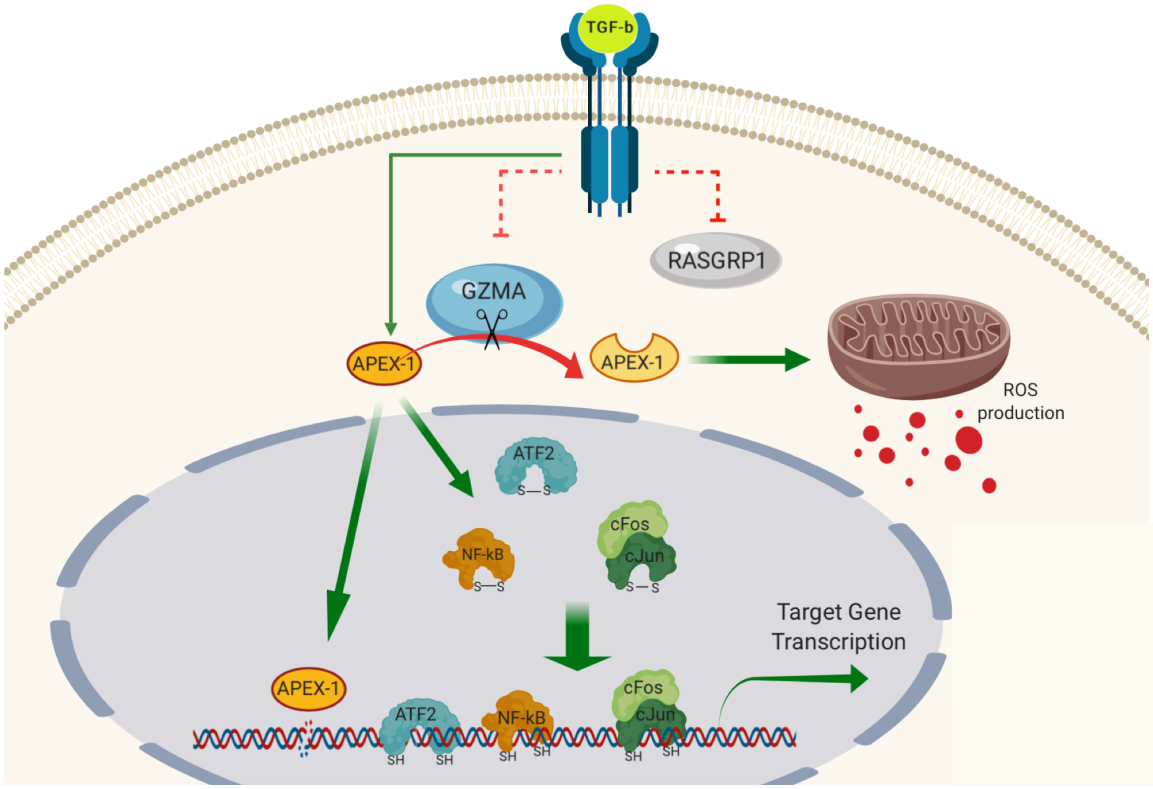

685 **Figure 6: Scheme of proposed TGF/GZMA/RASGRP1/APEX1 pathway**

In virulent hyper-disseminating macrophages enhanced TGF-β2 signaling results in upregulated *APEX1* transcription and suppressed *GZMA/RASGRP1* transcription. By contrast, in macrophages attenuated for dissemination reduced TGF-β2 signaling leads to lower *APEX1* transcription and increased in *GZMA* expression. Higher levels of GZMA cleave lower levels of APEX-1 ablating its oxidative repair functions leading to increased ROS output that typifies attenuated macrophages. In virulent, macrophages TGF-β2–induced APEX-1 reduces oxidized forms of target transcription factors such as NF-κB, ATF2, cFos and cJun to increase their DNA binding activity that augments transcription of their target genes to promote cellular transformation and tumor dissemination.

686 **Supplementary figure legends**

687 **Figure S1: Sequencing quality of all samples.**

688 (a) Clustering of all samples. (b) Density plot representing FPKM distribution of all
689 samples.

690 **Figure S2: Differentially expressed genes in TBL20, TBL3 and Attenuated Ode**
691 **leukocytes.**

692 (a) Histogram showing the number of up- (dark grey) and down- (light grey) regulated
693 genes in all 3 datasets. The area-proportional Venn diagrams represent the intersection
694 between the lists of DEGs from CuffDiff2 (green), DESeq2 (black) and baySeq (blue). The
695 intersection between the 3 pipelines reflects the number of up- and down-regulated
696 genes. The list of DEGs is listed in Table S2. (b) qRT-PCR confirmation of randomly
697 selected genes in TBL20 and TBL3. The reactions were set in 3 biological replicates and
698 the fold change calculating with the $2^{\Delta\Delta ct}$ method. The error bars represent SEM..

699 **Figure S3: Log2FC values of RASGRP1-4 in TBL20 and TBL3**

700 RNAseq Log2FC values from DESeq2 of TBL20 and TBL3 compared to BL20 and BL3,
701 respectively.

702 **Figure S4: Effect of *GZMA* knockdown on H_2O_2 output.**

703 H_2O_2 output by virulent (V), attenuated (A), and attenuated Ode macrophages after
704 CRISPR/Cas9-mediated *GZMA* knockdown. Error bars represent SD of 3 biological
705 replicates. ** and ## represent $p<0.01$ compared to virulent and attenuated Ode
706 macrophages, respectively.

707 **Figure S5: Effect of *RASGRP1* knockdown on *GZMA* expression.**

708 qRT-PCR of GZMA in virulent (V), attenuated (A) and attenuated Ode macrophages after
709 CRISPR/Cas9-mediated *RASGRP1* knockdown. Error bars represent SD of 3 biological
710 replicates *** and ### represent $p<0.001$ compared to virulent and attenuated Ode
711 macrophages, respectively.

712 **Figure S6: Schematic of *T. annulata* host cells and human cancer cell lines**
713 **transcriptome clustering**

714 **Figure S7: Complete cluster of 934 human cancer cell lines and BL20/TBL20,**
715 **BL3/TBL3**

716 **Table S1: Top 5 up- and down-regulated DEGs in infected and attenuated cell lines.**

717 This list was generated based on FC values of DEGs listed in Table S2.

718 **Table S2: List of DEGs in infected and attenuated cell lines.**

719 For details on the methods used to generate this list, please see in the materials and
720 methods section.

721 **Table S3: List of qRT-PCR primers.**

722 **Table S4: List of DEGs in attenuated Ode macrophages after TGF-β2 treatment.**

723 Genes listed as DE from DESeq2